Macrotransport-Solidification Kinetics Modeling of Equiaxed Dendritic Growth: Part I. Model Development and Discussion

L. NASTAC and D.M. STEFANESCU

An analytical model that describes solidification of equiaxed dendrites has been developed for use in solidification kinetics-macrotransport modeling. It relaxes some of the assumptions made in previous models, such as the Dustin–Kurz, Rappaz–Thevoz, and Kanetkar–Stefanescu models. It is assumed that nuclei grow as unperturbed spheres until the radius of the sphere becomes larger than the minimum radius of instability. Then, growth of the dendrites is related to morphological instability and is calculated as a function of melt undercooling around the dendrite tips, which is controlled by the bulk temperature and the intrinsic volume average concentration of the liquid phase. When the general morphology of equiaxed dendrites is considered, the evolution of the fraction of solid is related to the interdendritic branching and dynamic coarsening (through the evolution of the specific interfacial areas) and to the topology and movement of the dendrite envelope (through the tip growth velocity and dendrite shape factor). The particular case of this model is the model for globulitic dendrite. The intrinsic volume average liquid concentration and bulk temperature are obtained from an overall solute and thermal balance around a growing equiaxed dendritic grain within a spherical closed system. Overall solute balance in the integral form is obtained by a complete analytical solution of the diffusion field in both liquid and solid phases. The bulk temperature is obtained from the solution of the macrotransport-solidification kinetics problem.

I. INTRODUCTION

SIMULATION of casting solidification has lately received increased attention because of the potentially significant savings in the time required for prototyping and in the cost associated with defective castings. The most recent breakthrough was the incorporation of solidification kinetics models in macrotransport codes. A second generation of computer models for solidification, the macrotransport-solidification kinetics (MT-SK) codes, has been launched and applied by a few progressive foundries. This resulted in increased accuracy of model prediction, as well as in an increased number of predictors, such as amount and spacing of phases, grain size, microstructural transitions, *etc.* While MT-SK modeling of solidification of eutectic alloys has found an early satisfactory solution,[1,2] equiaxed dendritic solidification has proven more difficult to tackle. This is not surprising, considering the complicated geometry of dendrites. Maxwell and Hellawell[3] have presented a model for the nucleation and the initial stages of solidification of spherical grains. Dustin and Kurz[4] developed a model in which heterogeneous nucleation, solute, and thermal undercooling were considered. Although their model predicts interesting features such as grain number and recalescence, it ignores the overall solute balance and assumes that the internal volume fraction of solid is constant during growth. Rappaz and Thevoz[5] have proposed a model based on solute diffusion in the liquid, heat, and solute balances, and diffusion-controlled growth kinetics. They assumed no back diffusion, complete mixing of solute within the interdendritic liquid, and ignored the role of thermal undercooling in growth kinetics.

The main goal of this research effort was to develop a model for equiaxed dendritic solidification that capitalizes on previous models, but relaxes some of their most restrictive assumptions. Indeed, in the case of relatively high cooling rates and large grain size, the thermal undercooling might become an important factor. In addition, even for substitutional elements, where the solute-solid diffusivity is very small, back diffusion has to be included to satisfy the overall mass balance equation. This is particularly important in the last stage of solidification, when the solute-liquid diffusivity is less significant. For interstitially dissolved elements, *e.g.*, carbon in Fe-C alloys, kinetics models without diffusion in the solid phase would considerably overestimate the growth of dendrites.

An important parameter in equiaxed dendritic solidification is the internal fraction of solid. Some models[4] assume a constant internal fraction, until the primary dendrite tips of adjacent grains come into contact (dendrite coherency), after which coarsening of secondary dendrite arms occurs to the end of solidification. Other models[2,5] relate the internal fraction of solid directly to solutal supersaturation, neglecting the curvature and thermal undercooling. Again, when coherency occurs, coarsening is calculated through Scheil's equation. Other models[5,6] calculate the fraction of solid directly from the heat balance, assuming uniform temperature within the grain and considering again only the solutal undercooling. These models relate the interface temperature variation only to the interface concen-

L. NASTAC, formerly Graduate Research Assistant, Department of Metallurgical and Materials Engineering, The University of Alabama, is Senior Staff Engineer, Concurrent Technologies Corporation, Johnstown, PA 15904. D.M. STEFANESCU, University Research Professor and Director of the Solidification Laboratory, is with the Department of Metallurgical and Materials Engineering, The University of Alabama, Tuscaloosa, AL 35487.

Manuscript submitted March 11, 1996.

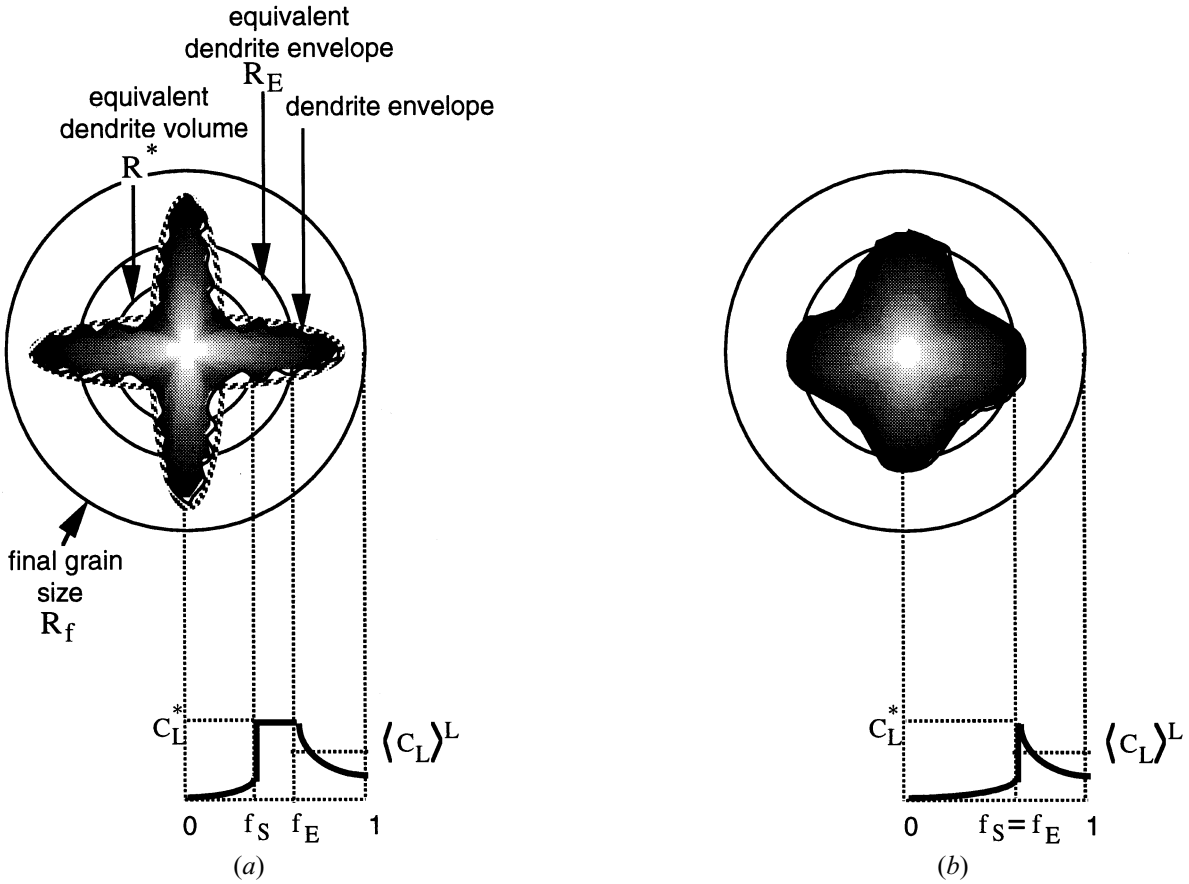

Fig. 1—Assumed morphologies and associated concentration profiles of solidifying equiaxed dendrites: (*a*) star dendrite (f_E variable) and (*b*) globulitic dendrite (f_E constant).

tration. However, if one assumes uniform temperature within the whole grain, *i.e.*, the interface temperature is equal to the bulk temperature, uniform concentration in the grain is imposed. The challenge is to simultaneously relate the internal fraction of solid to the movement of the dendrite tips, driven by the local undercooling in the liquid adjacent to the tip, and to the dynamic coarsening of dendrite arms occurring concurrently with the growth of dendrites.

A second goal of this work was to incorporate the solidification kinetics model for growth of equiaxed dendrites into a macrotransport solidification code. This MT-SK code could then be used for validation on shaped castings made of commercial alloys.

For the case of no convective transport, macroscopic modeling involves the solution of the heat-conduction equation subject to appropriate boundary conditions:

$$\rho c_p\,(T)\,\frac{\partial T}{\partial t} = \nabla[K(T)\,\nabla T] + Q \quad \text{with } \dot{Q} = \rho L\,\frac{\partial f_S}{\partial t} \qquad [1]$$

where T is the temperature, K is the thermal conductivity, ρ is the density, c_p is the specific heat, $\dot{Q}$ is the source term associated with the phase change, which describes the rate of latent heat evolution during the liquid/solid transformation, L is the latent heat of fusion, and f_s is the fraction of solid. Micromodeling essentially relies on the application of nucleation and growth kinetics laws to the derivation of the time evolution of solid fraction that is explicitly coupled with the heat-conduction equation through the source term $\dot{Q}$.

II. MODEL DEVELOPMENT

To build a MT-SK model for casting solidification, it is necessary to develop a methodology for the calculation of the evolution of the fraction of solid, and then to couple this evolution with the governing macrotransport equations. Such an approach has been previously discussed in the literature for eutectic alloys,[1,7,8] as well as for dendritic alloys.[1,2,5,9]

Consider a spherical volume element, v_f, within a liquid multicomponent alloy. A spherical nucleus of radius R_n grows, develops surface instabilities, and eventually fills the whole volume element. The assumed geometry and the solute concentration profiles developed in the solid and liquid phases for one of the elements are presented schematically in Figure 1. Solidification begins when the radius of the solid is that of the critical nucleus, $r = R_n$. At the nucleation temperature $T_n \le T_L$, the first solid formed has a solute concentration kC_0, where k is the equilibrium partition coefficient at the interface. It is considered that the unconstrained growth of the equiaxed dendritic grain is controlled by the thermal and solutal fields as well as by curvature.

The initial growth of the grains is assumed to be spherical (unperturbed sphere), until a critical size corresponding

to the onset of morphological instability is reached. Then, surface perturbations occur and dendritic growth starts. The growth of the dendrite is related to morphological instability and is calculated as a function of melt undercooling, which is controlled by the bulk temperature and the intrinsic volume average concentration in the liquid. Dynamic-coarsening kinetics of dendrite arms within the interdendritic region (mush) occurs simultaneously with dendritic growth. The coarsening process must be treated as dynamic since, as opposed to isothermal coarsening, it takes place as the fraction of solid increases and, therefore, within a liquid that changes composition. The driving force for the coarsening process is the difference in chemical potential (volume diffusion) of dendrite arms with different curvatures (interfacial energies). Once the diffusion fields around dendrite tips interact with those of neighboring dendrites, the dendrite tips stop growing. Then, only the coarsening process within the mushy zone causes the thickening of dendrites.

Two typical cases of dendrite morphology can be considered: ''star'' dendrites developed at low undercooling (Figure 1(a)), and ''globulitic'' dendrites growing at high undercooling (Figure 1(b)). The formation of these two different morphologies can be understood in terms of the driving force for growth that is active in the interdendritic space. When undercooling in the interdendritic space is small, higher order instabilities (secondary, tertiary, *etc.*, arms) would develop rather slowly, with the formation of star-type dendrite. On the other hand, if the undercooling is large, significant growth of higher order instabilities is to be expected, resulting in globulitic-type dendrite. The star dendrite is a single crystal consisting of six primary arms, one in each ⟨100⟩ direction of the dendritic crystal. Each primary arm has secondary arms, which in turn have tertiary arms. The number of secondary and tertiary arms increases rapidly with undercooling, eventually resulting in a globulitic dendrite. For a star dendrite, the volume fraction of solid f_S (equivalent dendrite volume, v_S) is smaller than that of the dendrite envelope f_E (equivalent dendrite volume v_E), as shown in Figure 1(a). For a globulitic dendrite, the volume fraction of solid is of the same order as the volume fraction of the dendrite envelope.

A. *Calculation of Solid-Fraction Evolution for the Star Dendrite*

Referring again to Figure 1(a), four different envelopes are defined:

(a) the dendrite envelope, which is the surface that includes the solid dendrite and the liquid between the secondary, and higher order dendrite arms;
(b) the equivalent dendrite envelope, (of radius R_E), which is the sphere having a volume equal to the volume enclosed by the dendrite envelope;
(c) the equivalent dendrite volume (of radius R^*), which is the sphere that has a volume equal to the solid dendrite; and
(d) the final grain size (of radius R_f), which is the sphere having a size equal to the maximum space allowable for dendrite growth; this is in fact the microvolume element.

From the foregoing, a number of fractions of solids can be defined:

$$f_S = \frac{v_S}{v_f} = \left(\frac{R^*}{R_f}\right)^3 \quad \text{fraction of solid in the volume element}$$
$$f_E = \frac{v_E}{v_f} = \left(\frac{R_E}{R_f}\right)^3 \quad \text{fraction of mush in the volume element} \qquad [2]$$
$$f_i = \frac{f_S}{f_E} \quad \text{internal fraction of solid}$$

Considering constant density and using the volume-averaging procedure,[10,11] the volume of solid in the mush (dendrite envelope) at any time during solidification can be calculated as

$$v_S = \int_{v_f} x_S \, dv = \sum_{j=1}^{N_i} v_S^j \qquad [3]$$

where x_S is the solid volume distribution function (that is, 1 for a point in the solid and 0 for a point in the liquid), v_f is the final grain volume, N_i is the number of instabilities (arms) at time t, and v_S^j is the solid volume of the instability.

Then, maintaining mass balance within the dendrite envelope (mush), all dendrite arms (primary and higher order) existing at one time for a given dendrite can be approximated as average instabilities that grow at the limit of their morphological stability, having the same total mass as the dendrite arms, but differing from them in number and size. Thus,

$$v_S = \sum_{j=1}^{N_i} v_S^j \cong \langle N\rangle_m^i \, \langle v\rangle_S^i \qquad [4]$$

where $\langle N\rangle_m^i$ is the average number of instabilities developed within the mush, and $\langle v\rangle_S^i$ is the average volume of the solid instability.

Dividing Eq. [4] by v_f and then differentiating it in time, the time evolution of the solid fraction, $\frac{\partial f_S}{\partial t}$ can be obtained as follows:

$$\frac{\partial f_S}{\partial t} = \frac{1}{v_f}\frac{\partial}{\partial t}\left(\langle N\rangle_m^i \, \langle v\rangle_S^i\right) = \frac{1}{v_f}\left(\frac{\partial\langle N\rangle_m^i}{\partial t}\langle v\rangle_S^i + \langle N\rangle_m^i \frac{\partial\langle v\rangle_S^i}{\partial t}\right) \qquad [5]$$

where $\frac{\partial\langle N\rangle_m^i}{\partial t}$ is the rate of creation of new instabilities, and $\frac{\partial\langle v\rangle_S^i}{\partial t}$ is the incremental volume change of an instability.

The number of instabilities $\langle N\rangle_m^i$ at time t and the final number of instabilities $\langle N\rangle_f^i$ can be calculated as follows:

$$\langle N\rangle_m^i = \frac{v_E}{v_f^i}\,\phi_C \qquad \text{and } \langle N\rangle_f^i = \frac{v_f}{v_f^i} \qquad [6]$$

where v_E is the volume of the mush (dendrite envelope), ϕ_C is a coarsening factor, and v_f^j is the final volume of instability. Inserting Eq. [6] into Eq. [5] and for constant ϕ_C, the fraction of solid evolution can be further obtained as follows:

$$\frac{\partial f_S}{\partial t} = \phi_C\left[\left(\frac{1}{v_f}\frac{\partial v_E}{\partial t}\right)\left(\frac{\langle v\rangle_S^i}{v_f^i}\right) + \left(\frac{v_E}{v_f}\right)\left(\frac{1}{v_f^i}\frac{\partial\langle v\rangle_S^i}{\partial t}\right)\right] \qquad [7]$$

In this equation, two length scales are involved: the scale of the equiaxed dendritic grain and the scale of instability.

Since $f_E = \frac{v_E}{v_f}$ (Eq. [2]), the evolution of solid fraction can be further written as

$$\frac{\partial f_S}{\partial t} = \frac{\partial f_E}{\partial t}\left(\frac{\langle v\rangle_S^i}{v_f^i}\,\phi_C\right) + f_E\left(\frac{\phi_C}{v_f^i}\,\frac{\partial\langle v\rangle_S^i}{\partial t}\right) \qquad [8]$$

As shown in previous models,[2–6] the fraction of solid can be defined as $f_S = f_E f_i$, where f_i is the internal fraction of solid. If this expression is differentiated in time and then compared with Eq. [8], term by term comparison shows that the internal fraction of solid can be described as

$$f_i = \frac{\langle v\rangle_S^i}{v_f^i}\,\phi_C = \frac{f_S}{f_E} \qquad [9]$$

This is a very important correlation between the evolution of instabilities and that of the dendrite envelope. In fact, the internal fraction of solid in Eqs. [8] and [9] couples the length scale of the dendrite with that of the instability. In the previous models, the length scale at the level of instability, *i.e.*, the dendrite arm scale, was neglected.

In order to develop a comprehensive model for the description of the evolution of solid fraction, additional constitutive and geometrical relations have to be defined. Accordingly, it is further assumed that there is no direct coupling between the solid instability and extradendritic liquid (outside the dendrite envelope); that is, a mushy zone (interdendritic region) develops such that the solid has only pointwise contacts with the extradendritic liquid (the dendrite tips). In this case, the interfacial area between the solid and liquid is nil, and

$$A_{Ld} = A_{dL} = A_E \qquad A_{Sd}^i = A_{dS}^i = A_S^i \qquad [10]$$

where A is the interfacial area, and the subscripts i, S, d, L, and E denote instability, solid, interdendritic liquid, extradendritic liquid, and dendrite envelope, respectively.

The shape factors of the instability, χ_S^i, and of the envelope, χ_E, are defined as

$$\chi_E = \frac{4\pi R_E^2}{A_E} \quad \text{and} \quad \chi_S^i = \frac{4\pi (r_S^i)^2}{A_S^i} \qquad [11]$$

where r_S^i is the position of the solid instability and R_E is the position of the equivalent dendrite envelope (Figure 1). Note that the shape factors defined in Eq. [11] are functions not only of the material under consideration but also of the undercooling or cooling rate. Usually, higher undercoolings produce larger shape factors (closer to unity).

The specific interfacial areas of the solid instability S_S^i and of the envelope S_E are

$$S_S^i = \frac{A_S^i}{v_f^i}\,\phi_C \qquad \text{and } S_E = \frac{A_E}{v_f} \qquad [12]$$

If the evolution of the volume dendrite envelope is approximated as $\frac{\partial v_E}{\partial t} = A_E\overline{V_E}$, and that of the instability as $\frac{\partial\langle v\rangle_S^i}{\partial t} = A_S^i\overline{V_S}$, it can be shown that the evolution of the fraction of solid of an equiaxed dendrite can be related to the interfacial area concentrations S_E and S_S^i as follows:

$$\frac{\partial f_S}{\partial t} = (S_E\,\overline{V_E})\,f_i + (S_S^i\,\overline{V_S})\,f_E \quad \text{with } S_E = \frac{1}{v_f}\,\frac{4\pi R_E^2}{\chi_E}$$
$$S_S^i = N_V^i\,\phi_C\,\frac{4\pi(r_S^i)^2}{\chi_S^i} \qquad \text{and } N_V^i = \frac{1}{v_f^i} = \frac{N_f^i}{v_f} \qquad [13]$$

where $\overline{V_E}$ is the average normal velocity of the dendrite envelope, $\overline{V_S}$ is the average normal velocity of the solid-interdendritic liquid interface, A_S^i is the surface area of instability, r_S^i is the radius of instability, and N_V^i is the volumetric density of instabilities. The term N_V^i can be calculated based on stereology[12] as

$$N_V^i = \frac{\pi N_A^2}{4N_L} \qquad [14]$$

where N_A and N_L are the areal and lineal densities, respectively.

The preceding expressions for the specific interfacial areas assume that the solid/liquid interfaces do not impinge upon each other. To take into account impingement during the late stages of solidification, an Avrami correction factor, $(1 - f_S)$, can be added to Eq. [13].

Equation [13] is the general expression for calculation of the evolution of solid fraction. It is related to the branching and coarsening by f_i, $\overline{V_S}$, χ_S^i, and r_S^i, to the number of instabilities by N_V^i or $\langle N\rangle_f^i$, and to the topology and movement of the dendrite envelope by χ_E, R_E, and $\overline{v}_E$. The first term in Eq. [13] describes the evolution of the dendrite envelope. The second term describes the coarsening (thickening) rate in the mush. If the dendrite envelope approaches the final grain size before complete solidification, $f_i = f_S$ and only coarsening in the mush will occur until the end of solidification or until the second-phase (usually eutectic or peritectic) transformation starts.

The specific interfacial areas S_E and S_S^i must be calculated through additional relations, either based on theoretical considerations or developed from experiments. Physically, they include the correct information regarding the geometry of the interfacial structures, and are thus related to complex multiscale phenomena, such as growth of various solid microstructures, impingement of interfaces, coalescence of grains, grain multiplication, and coarsening of dendrite arms (instabilities).

The specific interfacial area S is related to the specific surface area (surface-to-volume ratio) S_v by $S_v = S \cdot (1 - f)$, where f is the volume fraction of the microstructure under consideration. The term S_v can be related to certain dendrite spacing, nuclei density, and time.[6] The term S is time dependent through coarsening (that is occurring independently of growth of the dendrite tip) at the scale of instability, and, generally, through the various volume fractions that are also functions of time.

In this work, by using Eqs. [9] and [13], S_S^i can be directly related to the internal fraction of solid and the radius of instability as

$$S_S^i = \frac{f_i}{r_S^i}\,\frac{3}{\chi_S^i} \qquad [15]$$

Equation [13] can be further simplified by using the two-scale coupling equation, Eq. [9]:

$$\frac{\partial f_S}{\partial t} = 3 f_S \left(\frac{\overline{V}_E}{R_E} \frac{1}{\chi_E} + \frac{\overline{V}_S}{r_S^i} \frac{1}{\chi_S^i} \right) \quad \text{with } f_S = \int_0^t \frac{\partial f_S}{\partial t}\, dt \qquad [16]$$

Equation [16] is valid until impingement of growing grains occurs. Note that the coarsening factor has disappeared in Eq. [16]. The first term in Eq. [16] involves calculations at the dendrite length scale. The second term includes calculations at the instability length scale and describes both formation and coarsening of instabilities.

The movement of the envelope ($\overline{V}_E$) is directly related to the kinetics of the various dendrite tips, which is discussed in more detail in Section II–C. The position of the equivalent dendrite envelope is calculated as follows:

$$R_E = \int_0^t \overline{V}_E\, dt \quad \text{until } R_E = R_f \qquad [17]$$

where the final equiaxed grain radius R_f is

$$R_f = \left[\frac{4\pi}{3} \cdot N_V (x,y,z) \right]^{-1/3} \qquad [18]$$

Here, N_V is the number of grains per unit volume (volumetric grain density), and x, y, and z, are the coordinates of the microelement within the macrosystem.

Let us now discuss the variables in Eq. [16]. Considering coarsening and growth (thickening) of spherical instabilities, the shape factor of instability χ_S^i is taken to be one. The shape factor for the dendrite envelope can be calculated assuming that the dendrite envelope preserves a cubic shape that encloses a growing sphere, that is, the equivalent dendrite envelope shown in Figure 1. In this way, it can be shown that the shape factor of the dendrite envelope is simply $\chi_E = \frac{\pi}{6}$. With these assumptions, the only unknowns in Eq. [16] are $\overline{V}_S$ and r_S^i. They are related to coarsening and growth of instabilities. The additional constitutive relations required for the calculation of $\overline{V}_S$ and r_S^i will be shown in Section II–E.

Equation [16] is used to model the fraction of solid evolution. When the dendrite envelope radius R_E extends to the final grain radius R_f, $\overline{V}_E = 0$ and $f_E = 1$. Then, only the second term of the Eq. [16] contributes to the fraction of solid evolution until $f_S = 1$. When the bulk temperature is below the eutectic temperature, nucleation and growth of the eutectic phase begin. Growth competition between eutectic and dendritic phases occurs below the eutectic temperature to the end of solidification.

The particular case of this model is the calculation of solid fraction evolution for the globulitic dendrite.

B. *Calculation of Solid-Fraction Evolution for the Globulitic Dendrite*

For the particular case of a globulitic dendrite, Eq. [16] is used, assuming that f_i is constant. In this case, the second term of the Eq. [16] is zero. Physically, such an approach implies constant rates of creation and thickening of instabilities during solidification. Therefore, using $\chi_E = \frac{\pi}{6}$, the solid fraction evolution for globulitic dendrite is

$$\frac{\partial f_S}{\partial t} = f_S \left(\frac{18}{\pi} \frac{\overline{V}_E}{R_E} \right) (1 - f_S)^{f_S} \qquad [19]$$

The impingement factor $(1 - f_S)^{f_S}$ is introduced to take into account the effective surface interfacial area between the solid equiaxed dendritic grains and the liquid phase. The classic Avrami correction factor $(1 - f_S)$ was derived for the case of spherical grains, for which coherency occurs rather late, *e.g.*, at 0.74 fraction solid. However, since dendrites are not spheres, their coherency will occur considerably faster than that of spherical grains, i.e., when their dendrite envelopes collide. Accordingly, the impingement factor was modified to describe the onset of impingement at an earlier stage.

Unlike the Avrami correction factor, which must be used only during the late stages of solidification, the impingement factor in Eq. [19] is used from the beginning to the end of solidification. It becomes important when $f_S \geq 0.5$. If R_E extends to R_f before solidification is complete, $f_i = f_S$ and the fraction of solid evolution can be calculated using the coarsening model described in Section II–E. In the Dustin and Kurz model,[4] the internal solid fraction was assumed to be an unknown material constant. In the present globulitic model, the internal fraction of solid is implicitly included in Eq. [19], and thus need not necessarily be known for the calculation of the growth of globulitic dendrites.

C. *Calculation of the Interface Position*

At the beginning of growth, immediately after nucleation, the solid develops as a sphere (unperturbed sphere). At some point, perturbations will form on the surface of the sphere. Thus, the problem is now to evaluate not only R^*, but also the time at which the sphere will start losing its stability.

1. *Model for growth of the unperturbed sphere*

Mullins and Sekerka[13] found that the critical size at which morphological instabilities occur on a growing sphere is $R_c = 14\ \Gamma\ \Delta T^{-1}$, which is seven times the size predicted through the theory of critical nucleation. This corresponds to a radius of 1 to 2 μm. They also found that more severe instabilities, characterized by an increase, not only of the amplitude but also of the ratio of the maximum to minimum polar radii of the harmonic perturbation would occur for particle radii somewhat larger than R_c. Further, they showed that a sphere growing in the liquid would essentially remain unperturbed until its radius becomes three times R_c. The radius of the unperturbed sphere is calculated with the following equations (Appendix I provides details):

$$R^* = \left(\frac{\Omega_c}{\sqrt{\pi}} + \sqrt{\frac{\Omega_c^{\,2}}{\pi} + 2\Omega_c} \right) \sqrt{D_L\, t} \quad \text{where}$$

$$\Omega_c = \frac{\Delta T - \dfrac{2\Gamma}{R^*}}{(k-1)\left[m\, \langle C_L \rangle^L - \left(\Delta T - \dfrac{2\Gamma}{R^*} \right) \right]} \qquad [20]$$

where Ω_c is the solutal supersaturation, m is the slope of

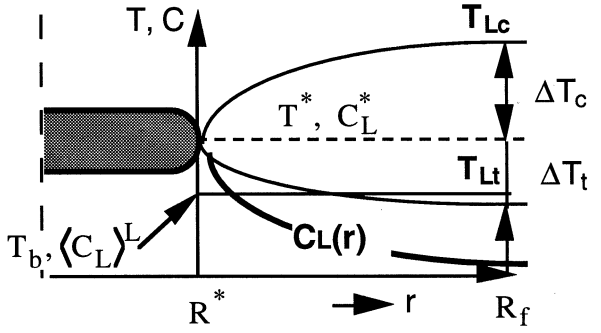

Fig. 2—Temperature and concentration fields and undercoolings at the dendrite tip.

the liquidus line, ΔT is the interface undercooling, Γ is the Gibbs–Thomson coefficient, D_L is the liquid diffusivity, k is the partition ratio, t is time, and $\langle C_L \rangle^L$ is the intrinsic volume average concentration.

2. *Model for growth of the equiaxed dendrite*

Two parameters, growth velocity, V and dendrite tip radius R, can be calculated by solving the thermal and diffusion field around the dendrite tip in conjunction with the stability criterion, as discussed in References 13 and 14. This implies that the dendrite will grow with a stable radius at the limit of its morphological stability. The simplest solution for the coupled problem of heat and mass transport at the dendrite tip is that suggested by Fisher (referred to in Reference 15) for the hemispherical dendrite tip. This solution also is applicable to both the thermal and solutal cases for a closed system.

The driving force for the dendrite growth is determined by the melt undercooling at the tip. If the curvature effect is introduced through the morphological stability criterion, as discussed hereafter, the total melt undercooling may be expressed as

$$\Delta T = \Delta T_c + \Delta T_t \qquad [21]$$

where the thermal undercooling is defined as $\Delta T_t = T^* - T_{Lt}(R_f)$ and the solutal undercooling as $\Delta T_c = T_{Lc}(R_f) - T^*$ (Figure 2). These two undercoolings can be evaluated through the Ivantsov transport solution in the first approximation form as

$$\Delta T = \Delta T_c + \Delta T_t = m\,(k-1)\,C_L^*\,\Omega_c + \frac{L}{c_p}\,\Omega_t \qquad [22]$$

where Ω_c and Ω_t are the solutal and thermal supersaturations, respectively, L is the latent heat of fusion, C_L^* is the interface liquid concentration, and c_p is the specific heat.

Using the hemispherical approximation, both supersaturations can be directly related to the solutal and thermal Peclet numbers as follows:

$$\Omega_c = Pe_c = \frac{VR}{2D_L} \quad \Omega_t = Pe_t = \frac{VR}{2\alpha_L} \qquad [23]$$

Growth velocity and tip radius can be coupled through the Mullins and Sekerka stability criterion as modified by Kurz and Fisher:[15]

$$R = \lambda_i = \sqrt{\frac{\Gamma}{\sigma^*\,(mG_c - G_t)}} \qquad [24]$$

Here, λ_i is the wavelength of instability of the solid-liquid interface, σ^* is a stability constant of the order of $(2\,\pi)^{-2}$, and G_c and G_t are the concentration and temperature gradients at the interface, respectively.

The concentration and temperature gradients at the tip of the dendrite are determined from the flux conditions at the interface to be

$$G_c = \frac{\partial C_L\,(R^*)}{\partial r} = \frac{VC_L^*(k-1)}{2D_L} \quad G_t = \frac{\partial T_L\,(R^*)}{\partial r} = -\frac{V\rho L}{2K_L} \qquad [25]$$

where R^* is the interface position, ρ is the density, and K_L is the liquid thermal conductivity. These gradients are related to the undercoolings through the Peclet numbers as

$$mG_c = \frac{\mathrm{Pe}_c}{R}\,m\,(k-1)\,C_L^* = \frac{\Delta T_c}{R} \quad G_t = -\frac{\mathrm{Pe}_t}{R}\,\frac{L}{c_p} = -\frac{\Delta T_t}{R} \qquad [26]$$

Substituting Eqs. [26] into Eq. [24] results in

$$R = \frac{\Gamma}{\sigma^*\,\Delta T} \qquad [27]$$

Finally, a mean growth velocity of the dendrite tip $\overline{V}_E$, driven by both the intrinsic volume average interdendritic and extradendritic liquid concentrations, can be calculated by substituting Eqs. [23] and [27] into Eq. [22]:

$$\overline{V}_E = \mu\Delta T^2 \quad \text{with } \mu = \frac{2\sigma^*}{\Gamma}\left[\frac{m(k-1)\,\langle C_d\rangle^d}{D_L} + \frac{\rho L}{k_L}\right]^{-1} \qquad [28]$$

where $\langle C_d \rangle^d$ is the intrinsic volume average interdendritic liquid concentration.

The melt undercooling for the system under consideration can be calculated based on the following definition/assumption (Figure 2):

$$\Delta T = T_L + m[\langle C_L\rangle^L - C_0] - T_b = T_m + m\,\langle C_L\rangle^L - T_b \qquad [29]$$

where T_L is the equilibrium liquidus temperature, T_m is the melting temperature of the pure metal, T_b is the bulk temperature defined as the average temperature in the volume element, and $\langle C_L \rangle^L$ is the intrinsic volume average extradendritic liquid concentration. Equation [29] includes both thermal and solutal undercoolings.

D. *Calculation of Solute Redistribution*

The model for solute redistribution used in the calculation of the equiaxed dendritic growth is a modified version of that recently published by the authors.[16] The main model assumptions include the following: solute transport in both phases is by Fickian diffusion, free movement of the solid-liquid interface, which is planar and under local equilibrium, and there is no solute flow into or out of the volume element. Overall mass balance is used to couple the concentration field in the extradendritic liquid, interdendritic liquid, and solid. In order to circumvent the difficulties that may arise in the calculation of solid-liquid interface concentrations, well-mixed interdendritic liquid was assumed (Figure 1), *i.e.*, $\langle C_d \rangle^d = C_L^*$. This is in line with Reference 6, where it was shown that the diffusion length of the interdendritic liquid is of the order of secondary spacing (here, instability spacing) and can be neglected at the scale of the whole grain. Considering a closed system and

constant densities (this is to simplify notations), the overall mass balance can be written as

$$C_0 v_f = \int_0^{R^*} 4\pi r^2\, C_S\,(r,t)\, dr + C_L^*\,(v_E - v_S) + \int_{R_E}^{R_f} 4\pi r^2\, C_L\,(r,t) dr \quad [30]$$

where C_0 is the initial concentration, t is time, and r is the radial coordinate.

The solute redistribution model allows calculation of the interface liquid concentration $C_L^*(t)$ and of the local concentration in the extradendritic liquid $C_L(r,t)$. The interface liquid concentration is given by the following equation:

$$C_L^* = C_0 \left[1 - \frac{(1-k) f_S}{1 - 3\,[kI_S + I_L]}\right]^{-1} \quad \text{with}$$
$$I_S = \frac{2 f_S}{\pi^2} \sum_{n=1}^{\infty} \frac{1}{n^2} \exp\left[-\left(\frac{n\pi}{f_S^{1/3}}\right)^2 \frac{D_S t}{R_f^2}\right] \quad \text{and} \quad [31]$$
$$I_L = 2 f_E^{2/3}\,(1 - f_E^{1/3}) \sum_{n=1}^{\infty} \frac{1}{\alpha_n^2} \exp\left[-\left(\frac{\alpha_n}{1 - f_E^{1/3}}\right)^2 \frac{D_L t}{R_f^2}\right]$$

where α_n is the *nth* root of the equation $\alpha_n/\tan(\alpha_n) = 1 - f_E^{1/3}$ and $f_E = \left(\frac{R_E}{R_f}\right)^3$.

The intrinsic volume average concentration $\langle C_L\rangle^L$ is obtained by integrating the local concentration over the extradendritic liquid phase. The solution of the local liquid concentration was taken from Reference 16. The only difference consists of interchanging the radius of the equivalent dendrite volume R^* with the radius of the equivalent dendrite envelope R_E.

$$\langle C_L\rangle^L = \frac{4\pi}{v_L} \int_{R_E}^{R_f} r^2\, C_L\,(r)\, dr = C_L^* + 6(C_0 - C_L^*) R_E^2 \frac{R_f - R_E}{R_f^3 - R_E^3} \sum_{n=1}^{\infty} \frac{\exp(-\lambda_n D_L t)}{\alpha_n^2} \quad [32]$$

where v_L is the volume of liquid phase and λ_n is $\lambda_n = \alpha_n^2 (R_t - R_E)^{-2}$.

E. *Growth and Coarsening of Instabilities*

The second term in Eq. [20] is based on the creation rate and thickening of spherical instabilities. It is assumed that the rate of creation and growth of instabilities occurs until $R_E = R_f$. Thereafter, the liquid between instabilities becomes solid based on a spherical coarsening model. The spherical instabilities grow at the limit of morphological stability with a morphological radius given by Eq. [27], *i.e.*, $r_S^i = r_0^i = R = \frac{\Gamma}{\sigma^*}\frac{1}{\Delta T}$. Thus, when thickening of instability is neglected, *i.e.*, during the creation period, the second term in Eq. [16] can be calculated as

$$\frac{\overline{V}_S}{r_s^i} = \frac{1}{r_s^i}\frac{\partial r_S^i}{\partial t} = -\frac{1}{\Delta T}\frac{\partial \Delta T}{\partial t} \quad [33]$$

where $\frac{\partial \Delta T}{\partial t}$ is the variation of the cooling rate at the *S/L* interface of instability.

A coarsening (thickening) model for spherical instabilities is derived in Appendix II. It is supposed that the coarsening mechanism is analogous to Oswald ripening of precipitates. The coarsening model follows some of the assumptions used in References 17 through 20. The model considers the dynamic nature of the spherical coarsening process through the fraction of solid evolution and time variation of liquid concentration in the mush. The mechanism of coalescence of instabilities is ignored in this model. The final result is

$$\overline{V}_S = \frac{\partial r_S^i}{\partial t} = \frac{0.75}{(r_S^i)^2}\frac{A}{\langle C_d\rangle^d}\frac{f_i^{1/3}}{(1 - f_i^{1/3})} \quad \text{with}$$
$$f_i = \frac{\langle v\rangle_S^i}{v_f^i}\,\phi_C = \left(\frac{r_S^i}{\lambda/2}\right)^3 \quad [34]$$

where λ is the average spacing between instabilities (at time t) and $A = \frac{D_L \Gamma}{m(k-1)}$.

To compare the present model with other coarsening models, Eq. [34] is written in terms of λ. Assuming that during solidification, the instantaneous rate of coarsening is identical to the isothermal rate of coarsening, *i.e.*, $\frac{1}{\lambda}\frac{\partial \lambda}{\partial t} = \frac{1}{r_S^i}\frac{\partial r_S^i}{\partial t}$, Eq. [34] can be written as

$$\lambda^2 \frac{\partial \lambda}{\partial t} = \frac{6A}{\langle C_d\rangle^d f_i^{2/3}\,(1 - f_i^{1/3})} \quad \text{or}$$
$$\frac{1}{\lambda}\frac{\partial \lambda}{\partial t} = \frac{6A}{\langle C_d\rangle^d \lambda^3 f_i^{2/3}\,(1 - f_S^{1/3})} \quad [35]$$

Thus, under this assumption, Eq. [35] is the same with the dynamic coarsening model developed by Mortensen[21] when f_i and 6 in Eq. [35] are replaced in Eqs. [10] and [15] from Reference 21 by f_s and 4.5, respectively.

When $R_E = R_f$, $f_i = f_s$ and the fraction of solid evolution is calculated using Eqs. [34], [35], and the second term of Eq. [16] as

$$\frac{\partial f_i}{\partial t} = \frac{\partial f_S}{\partial t} = \frac{f_S^{4/3}}{(1 - f_S^{1/3})}\frac{18A}{(r_S^i)^3}\frac{1}{\langle C_d\rangle^d} = \frac{f_S^{1/3}}{(1 - f_S^{1/3})}\frac{18A}{\lambda^3}\frac{1}{\langle C_d\rangle^d}$$

with

$$\overline{r}_0^i = \frac{3}{R_E - R_n}\int_{R_n}^{R_E} \frac{\Gamma}{\sigma^*\,\Delta T}\, r^2\, dr \quad [36]$$

In Eq. [36], $^-r_0^i$ is the average tip radius over the dendrite envelope and is calculated at the onset of coarsening. Equation [36] gives information about the evolution of both fraction of solid and spacing between instabilities.

III. DISCUSSION

A. *Calculation of Specific Interfacial Areas*

The time evolution of the specific interfacial area during solidification also may be evaluated experimentally. Using

stereological calculations,[12] S_v can be obtained from $S_v = (4 / \pi) \cdot L_A = 2 \cdot P_L$, where L_A is the sum of lengths of linear features divided by total test area (perimeter) and P_L is the number of point intersections per unit length of test line.

It was also shown[22,23,24] that S_s can be associated with the permeability K_p of the porous envelope. The permeability can be experimentally measured or it can be estimated from the Kozeny–Carman model.[23,25]

B. *Multiscale Interactions in Equiaxed Dendritic Growth*

Using $\langle C_L \rangle^L$ rather than $C_L(R_f)$ that was used in Reference 5, the overall mass balance is satisfied. Also, the interaction between instabilities around the dendritic grain is approximated.[5,25] The term $\langle C_d \rangle^d$ is used to take into account the interaction among instabilities in the interdendritic region. Generally, each dendrite tip (primary, secondary, *etc.*) moves at a different speed, depending on the local undercooling in the liquid adjacent to the tip. Since growth of average instabilities is considered, a mean dendrite tip velocity can be uniquely related to the average undercooling in the extradendritic liquid, *i.e.*, Eq. [29]. In fact, this is the main advantage of using the averaging method, in that it allows calculation at multiscale level.

C. *Equiaxed Dendritic Growth in Multicomponent Systems*

Assuming that the influence of various elements on the liquidus slope and partition coefficient can be obtained from mass weighted average, for a multicomponent system, the growth coefficient μ can be modified as follows:

$$\mu = 2\ \sigma^* \left\{ \sum_{i=1}^{n} \left[\Gamma_i \left(\frac{m_i\ (k_i - 1)\ C_{L_i}^{*2}\ \rho_i}{D_{L_i} \sum_{j=1}^{n} C_{L_j}^{*}\ \rho_j} + \frac{\rho L}{K_L} \right) \right] \right\}^{-1} \qquad [37]$$

where n is the number of components in the alloy. Similarly, the undercooling can be evaluated with

$$\Delta T = T_m + \sum_{i=1}^{n} m_i\ \langle C_{L_i} \rangle^L - T_b \qquad [38]$$

This is valid in particular for low concentration of the components (<1 pct), when it is assumed that the interactions among various alloying elements can be neglected.[26–32] It should also be noted that the stability constant σ^* may vary with concentration.[33]

D. *Analysis of the Equiaxed Dendritic Growth Model*

The analysis was conducted in two stages. First, a calculation was performed to compare hemispherical (first approximation of the Ivantsov's solution) *vs* parabolic (fully Ivantsov's solution) growth of the dendrite tip. Second, the proposed model for growth velocity of the tip of the equiaxed dendrite was checked against literature experimental data on succinonitrile (SCN).

1. *Parabolic vs hemispherical growth of the dendrite tip*

In the present context, a hemispherical dendrite tip was assumed. This is the first approximation of the Ivantsov transport solution. A parabolically shaped dendrite tip also can be assumed. In this case, the complete Ivantsov's solution has to be applied.[34,35] However, the shape of the dendrite tip radius is not necessarily paraboloidal. Indeed, as shown in Reference 36, the krypton dendrite tip observations at low undercoolings (perhaps due to convection) negate the existence of an Ivantsov profile and provide direct evidence for theories based on the stability analysis of a nearly spherical tip.

The influence of convection on the dendrite tip velocity also may be important. Large discrepancies appear for a parabolically shaped dendrite tip, when one compares the solution obtained by thermal convection theory with that obtained by Ivantsov's thermal-conduction theory.[37] Note that convection is always present in solidification of castings.

In spite of this controversy, the scope of present research is to establish a general framework (methodology) for the case of interacting equiaxed dendritic grains, whose growth is perturbed by the inadvertent interference of the thermal and solutal fields and of grain impingement that occurs toward the end of solidification. Under these conditions, the central issue revolves around mass, energy, and species conservation.

However, to check the validity of the hemispherical approximation against parabolic solution for the tip growth velocity an analysis was performed for an IN718 alloy.

a. *Hemispherical growth*

Assuming no thermal undercooling and hemispherical diffusion field at the dendrite tip, it can be shown that (Eq. [22]):

$$V = \frac{2\sigma^*}{\Gamma} \frac{D_L}{m\ (k-1) C_L^*} \Delta T^2 \quad \text{with} \quad \Delta T = \Delta T_c = m\ (\mathrm{k} - 1) C_L^*\ \Omega_c \qquad [39]$$

where

$$\text{where } \Omega_c = \frac{C_L^* - C_0}{C_L^* (1-k)} = \mathrm{Pe}_c = \frac{VR}{2D_L} \quad \text{and} \quad C_L^* = \frac{1}{1 - (1-k)\ \mathrm{Pe}_c} \qquad [40]$$

Combining Eqs. [39] and [40] results in

$$VR^2 = \frac{2\Gamma}{\sigma^*} \frac{D_L}{m\ (k-1) C_0} [1 - (1-k)\ \mathrm{Pe}_c] \qquad [41]$$

Note that the hemispherical-tip growth velocity (V) in Eq. [41] can be exactly calculated by substituting $\mathrm{Pe}_c = \frac{V\,R}{2D_L}$ and solving for V.

b. *Parabolic growth*

From Reference 35, Eq. [A8.17], neglecting the thermal undercooling, the following equation can be directly obtained:

$$R = \frac{\Gamma}{\sigma^*} \frac{D_L}{\mathrm{Pe}_c\ m\ (k-1)\ C_0} [1 - (1-k)\ Iv\ (\mathrm{Pe}_c)] \qquad [42]$$

where $Iv(\mathrm{Pe}_c)$ is the Ivantsov's function. Since $\mathrm{PE}_c = \frac{V\,R}{2D_L}$ the parabolic growth equation is

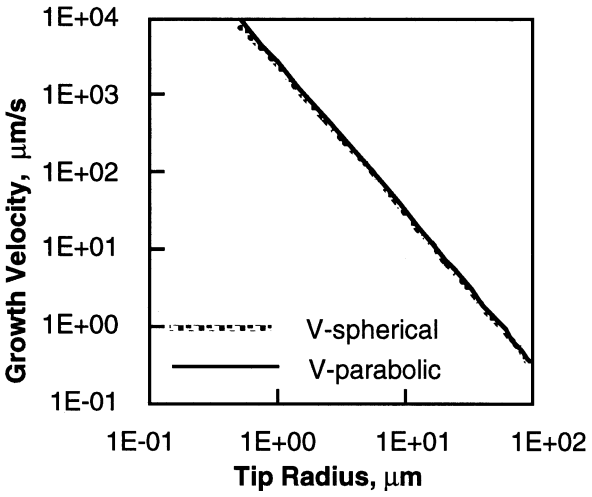

(*a*)

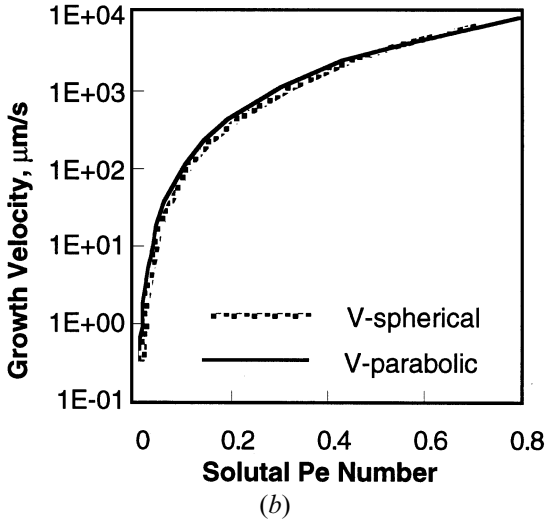

(*b*)

Fig. 3—Comparison between hemispherical and parabolic tip growth velocities as a function of (*a*) tip radius and (*b*) solutal Pe number.

$$VR^2 = \frac{2\Gamma}{\sigma^*} \frac{D_L}{m\,(k-1)\,C_0} [1 - (1-k)\,Iv\,(\mathrm{Pe}_c)] \quad [43]$$

The parabolic tip growth velocity in Eq. [43] was solved through an iterative method. Note that Pe_c in Eq. [41] is replaced by the Ivantsov's function in Eq. [43]. This is the only difference between two models.

c. *Comparison between hemispherical and parabolic growth*

Although there is a significant difference between the hemispherical approximation and the parabolic solution in terms of Peclet number,[35] small discrepancies are observed when growth velocities *vs* either tip radius or solutal Peclet number are plotted. Some calculations were made for INCONEL* 718 using the data given in Reference 38. The results are presented in Figure 3.

The range of cooling rates used in this analysis is between 0.1 to 10,000 μm/s (that corresponds to the variation of the Peclet number from 0.001 to 1.0 and of the tip radius from 0.2 to 100 μm). Usually, the range of growth velocities encountered in castings is between 0.1 to 1,000 μm/s. This corresponds to a variation of Peclet number from 0.001 to 0.50 and of tip radius from 1 to 100 μm. The maximum solutal Pe number used in the present model is 0.5. For this range of Pe numbers, the error is maximum 5 pct.

Because the Ivantsov's solution of the tip velocity gives tremendous difficulties in multiscale coupling and in solving the interface liquid concentration in parabolic coordinates, the hemispherical approximation for the tip was adapted in the present model.

d. *Comparison between calculated and experimental growth velocities of dendrite tip for succinonitrile*

In many contemporary casting solidification models, dendrite kinetics is calculated assuming a parabolic dendrite tip, while the diffusion field is calculated using spherical coordinates. This is not consistent. A more correct approach would be to use a hemispherical dendrite tip in conjunction with spherical coordinates for diffusion calculation. However, there is an ongoing discussion on the relative merits of the parabolic tip over the hemispherical tip. To verify calculation accuracy or lack of it when using a hemispherical tip, we selected a classic experiment performed on succinonitrile.[39]

This particular experiment was conducted isothermally, in a large bath (infinite domain). Since Eqs. [27] and [28] describe the nonisothermal solidification into a closed system, two changes were made in these equations. First, the intrinsic volume average concentration of the liquid phase was assumed to be equal to C_0, consistent with the infinite domain. Second, the interface-liquid concentration was obtained from the hemispherical approximation (second part of Eq. [40]). The thermophysical parameters of succinonitrile used in calculations are those listed in References 34, 35, and 39.

The growth velocity for succinonitrile—0.07 mole pct impurity (assumed to be acetone)—calculated with the present modified mode is compared with experimental values in Figure 4. The model compares favorably with the experimental data, in particular in the region of moderate velocities, which are typical for castings. The discrepancy shown in Figure 4 at low undercooling probably may be diminished by including thermal convection calculations.[37]

E. *Dendrite coherency*

Dendrite coherency occurs when dendrite tips of adjacent grains come into contact, *i.e.*, when $R_E = R_f$. It is one of the most important parameters used to establish the rheology of a particular system. Since it is dependent on the evolution of the dendrite envelope, all factors that augment the evolution of envelope fraction, such as topology and movement of envelope, should reduce the dendrite coherency.

The purpose of the following analysis is to evaluate the influence of some process and material parameters on the onset of dendrite coherency. The alloy selected for this analysis is an Fe-0.6 pct C. The data used in calculation are given in Table I. These are typical data as found, for example, in Reference 18.

*INCONEL is a trademark of INCO Alloys International, Huntington, WV.

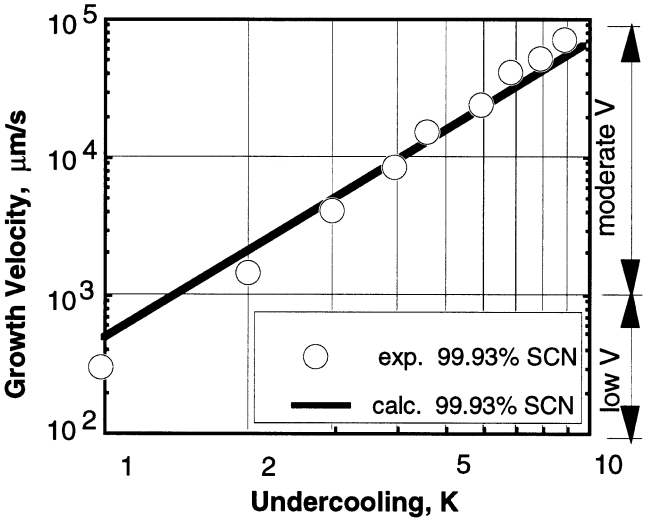

(*a*)

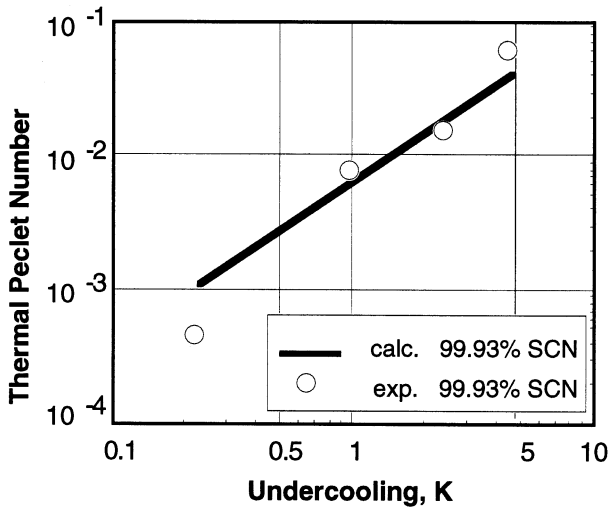

(*b*)

Fig. 4—Comparison of data calculated with the present model and experimental data on succinonitrile obtained by Glicksman *et al.*[39] The concentration is measured in mole percent.

The evolution of envelope fraction and internal fraction of solid during solidification of the Fe-0.6 pct C alloy for a cooling rate of 4 °C/s was calculated using the model for the growth of the star dendrite, described in Section II. The results are presented in Figures 5 and 6.

From Figure 5(a), it can be seen that coherency is calculated to occur for an envelope fraction of one. For this particular cooling rate, coherency occurs at 0.55 fraction solid, when the internal fraction of solid becomes equal to the fraction of solid. Figure 5(b) shows the dendrite coherency during solidification of the same alloy as a function of cooling rate. It is seen that for the range of cooling rates selected for this analysis, the onset of coherency moves to higher fraction solid as the cooling rate decreases.

To evaluate the influence of the diffusion model on the onset of coherency, the interface liquid concentration was calculated using Scheil, equilibrium, and Eqs. [31] and [32]. Then, the proposed model was used to obtain data on the onset of coherency and on the solidus temperature for these three different assumptions on microdiffusion calculations. The results presented in Table II indicate that equilibrium calculation results in the higher coherency, while Scheil predicts the lower coherency. The present model, as expected, predicts an intermediate coherency because it accounts for back diffusion.

In Figure 6, the complex influence of the cooling rate on equiaxed dendritic growth is presented. The cooling rate was calculated immediately above the liquidus temperature. In Figure 6(a) it is seen that as the cooling rate increases, recalescence first increases and then disappears. The cooling rate also affects grain size and the onset of coherency, as shown in Figure 6(b).

The model has been incorporated in a commercial macrotransport code for modeling of casting solidification (PROCAST). Computation details and experimental validation performed on INCONEL 718 castings are described in Part II of this article.

IV. CONCLUDING REMARKS

A new analytical model for calculation of the evolution of fraction of solid during solidification of alloys with equiaxed dendritic morphology has been developed. The initial growth of the grains is assumed spherical (unperturbed sphere) until a critical size corresponding to the onset of morphological instability is reached. Dendritic growth also is related to morphological stability, involves diffusion in both solid and liquid phases, and is controlled by thermal, solutal, and curvature undercooling. Coarsening during solidification, interaction, and coupling between different length scales involved in equiaxed dendritic growth, as well as the selection of the model for dendrite-tip growth velocity have been thoroughly discussed. Calculations for a Fe-0.6 pct C alloy demonstrate that the onset of coherency is a function of cooling rate. This calculation is sensitive to the assumptions made for microdiffusion. Indeed, a Scheil diffusion model predicts lower coherency than an equilibrium model. When a complete diffusion model is used, intermediate results are obtained, as expected.

APPENDIX I
Unperturbed spherical growth

Assuming that the spherical growth is due only to the mass diffusion in both solid and liquid phases, the velocity of the interface V can be calculated through mass balance at the interface as follows:

$$V(C_L^* - C_S^*) = - D_L \left.\frac{\partial C_L}{\partial r}\right|_{r=R^*} + D_S \left.\frac{\partial C_S}{\partial r}\right|_{r=R^*} \quad [Ia]$$

where the first derivatives can be obtained by derivation of the solutions of the diffusion equation presented in Reference 16 (based on the exact solution of the time-dependent ''Fickian'' diffusion equation) as follows:

$$\left.\frac{\partial C_L}{\partial r}\right|_{r=R^*} = - 2 \frac{C_L^* - C_0}{R_f - R^*} \sum_{n_L=1}^{\infty} \exp\left[-\lambda_{n_L} D_L t\right] \quad [Ib]$$

and

Table I. Data Used in Calculations of Fe-0.6 wt Pct C Alloy (γ Austenite)

D_S ($m^2\ s^{-1}$)	D_L ($m^2\ s^{-1}$)	k	C_{eut} (wt pct)	m_L (K wt pct^{-1})	T_L (°C)	T_{eut} (°C)	T_m (°C)	R_c (m)	R_n (m)
5×10^{-10}	2×10^{-9}	0.34	4.3	−80.0	1490.0	1155.0	1538.0	1×10^{-5}	1×10^{-6}

R_f (m)	L (J kg^{-1})	Γ (K m)	ρ (kg m^{-3})	K_L (W $m^{-1}\ K^{-1}$)	c_p (J $kg^{-1}\ K^{-1}$)
$2 \times 10^{-4} \times \dot{T}^{-0.5}$	270,000	1.9×10^{-7}	7300	30.0	800.0

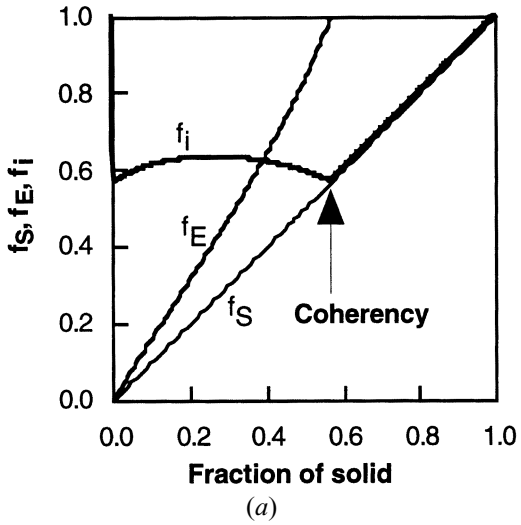

(*a*)

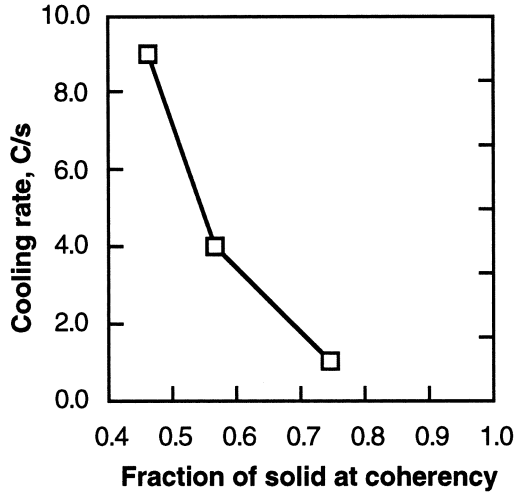

(*b*)

Fig. 5—Calculated evolution of the envelope fraction and internal fraction of solid for a cooling rate of 4 °C/s (*a*) and calculated dendrite coherency as a function of cooling rate (*b*) during solidification of an Fe-0.6 pct C alloy.

$$\left.\frac{\partial C_S}{\partial r}\right|_{r=R^*} = 2\ k\ \frac{C_L^* - C_0}{R^*} \sum_{n_S=1}^{\infty} \exp\left[-\lambda_{n_s} D_S t\right] \quad \text{with} \quad \lambda_{n_s} = \left[\frac{n\ \pi}{R^*}\right]^2 \qquad [\text{Ic}]$$

At very small interface radii, negligible interference between neighboring growth centers should be registered, and the composition of the bulk liquid should remain effectively C_0.[3] Consequently, the solutal supersaturation can be defined as

$$\Omega_c = \frac{C_L^* - C_0}{C_L^* - C_S^*} = \frac{C_L^* - C_0}{C_L^*\,[1 - k]} \qquad [\text{Id}]$$

By combining Eqs. [Ia] through [Id], the following expression is obtained for the growth velocity:

$$V = 2\ \Omega_c \left\{ \frac{D_L}{R_f - R^*} \sum_{n_L=1}^{\infty} \exp\left[-\lambda_{n_L} D_L t\right] - \frac{kD_S}{R^*} \sum_{n_S=1}^{\infty} \exp\left[-\lambda_{n_s} D_S t\right] \right\} \qquad [\text{Ie}]$$

While this is the exact solution of the problem, the use of this equation in calculations is cumbersome. Aaron *et al.*[40] have reviewed the mathematical analysis of the diffusion-limited spherical growth. They pointed out that for solutal supersaturation smaller than 0.3 (typical for equiaxed dendritic growth), the invariant-size approximation (stationary interface) would provide results in good agreement with their exact error function solution. For the invariant-size approximation the position of the interface can be calculated simply as

$$R^* = \lambda_D \sqrt{D_L t} \quad \text{where } \lambda_D = \frac{\Omega_c}{\sqrt{\pi}} + \sqrt{\frac{\Omega_c^2}{\pi} + 2\Omega_c} \qquad [\text{If}]$$

In the preceding models, curvature undercooling was ignored. However, the curvature undercooling cannot be neglected when considering the growth of small grains at small undercooling.[3] The curvature effect on the tip undercooling can be introduced as follows (refer to References 3, 14 and 15):

$$\Delta T = \Delta T_c + \Delta T_\Gamma = m\ (k - 1) C_L^*\ \Omega_c + \frac{2\Gamma}{R^*} \qquad [\text{Ig}]$$

where ΔT_Γ is the curvature undercooling. From Eqs. [29] and [Ig], the solutal supersaturation can be obtained as

$$\Omega_c = \frac{\Delta T - \dfrac{2\ \Gamma}{R^*}}{(\mathrm{k} - 1)\left[m\ \langle C_L \rangle^L - \left(\Delta T - \dfrac{2\ \Gamma}{R^*}\right)\right]} \qquad [\text{Ih}]$$

Since the growth velocity is small, in numerical calculations, the curvature undercooling can be calculated using the interface radius from the previous time-step. Note that the supersaturation calculated with Eq. [Ih] is equivalent to that obtained through Eq. [Id] under the assumption that the thermal undercooling is negligible at the beginning of solidification. Indeed, as shown in References 3 and 35, the

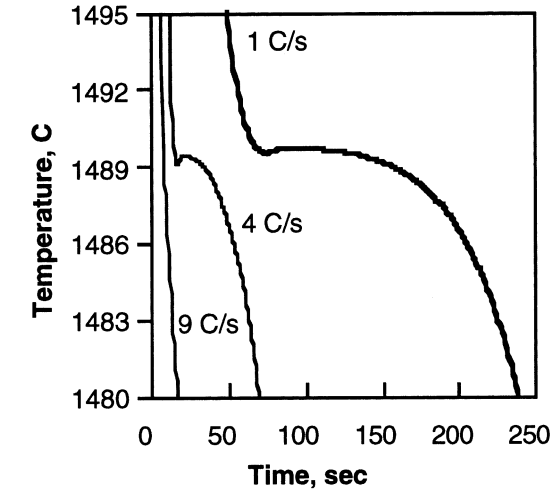

(*a*)

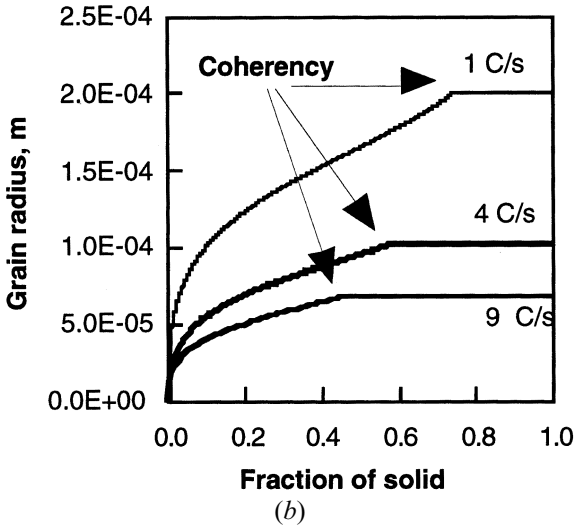

(*b*)

Fig. 6—Calculated cooling curves (*a*) and grain size evolution (*b*) during solidification of an Fe-0.6 pct C alloy.

Table II. Calculated Correlation between the Onset of Coherency, Final Liquid Concentration and Solidus Temperature with Three Different Assumptions for Microdiffusion Calculations (Fe-0.6 pct C alloy, 4 °C/s)

Diffusion Calculation	Scheil	Present Model	Equilibrium
Solid fraction at coherency	0.49	0.57	0.61
Final liquid concentration, wt pct	4.3	2.05	1.73
Solidus temperature, °C	1142	1377	1399

thermal undercooling for a growing unperturbed sphere may be neglected by comparison with solutal or curvature undercoolings.

Finally, the growth velocity of the interface (or the interface position) can be calculated with either Eq. [Ie] or [If] in conjunction with Eq. [Ih]. For a multicomponent system, the interface position can be obtained similarly from mass weighted average (Eqs. [37] and [38]).

APPENDIX II
A model for spherical coarsening (thickening) kinetics

The coarsening process is calculated in spherical coordinates. It is assumed that at any time, only two distributions of dendrite arms (instabilities) with two different radii need to be considered. The mean radius of the two instabilities is the radius of the considered average instability, *i.e.*, r_S^i. The thinner instability (of radius r) remelts and the thicker one (of radius R) grows. The mechanism of coalescence of instabilities is ignored in this model.

Assuming that the two instabilities are situated in a locally isothermal melt and local equilibrium is established very rapidly at the interface, the difference in curvature undercoolings (interfacial energy gradient) is equilibrated by the difference in solutal undercoolings (diffusion gradient). That is,

$$m\left(C_L^R - C_L^r\right) = 2\,\Gamma\left(\frac{1}{R} - \frac{1}{r}\right) \quad \text{with } r_S^i = \frac{R + r}{2} \qquad \text{[IIa]}$$

Assuming further that the radius of shrinking instability is half of the radius of growing instability, Eq. [IIa] is written in term of average instability as

$$m\,(C_L^R - C_L^r) = -\frac{1.5\,\Gamma}{r_S^i} \qquad \text{[IIb]}$$

Further, an average flux balance existing between instabilities can be written as

$$D_L\frac{(C_L^R - C_L^r)}{d} = C_L^*(1 - k)\frac{\partial r_S^i}{\partial t} \quad \text{with} \quad d = 2\,(\lambda/2 - r_S^i) \qquad \text{[IIc]}$$

where λ and d are the average spacing and average distance between instabilities, respectively.

Combining Eqs. [IIb] and [IIc] and replacing C_L^* with average interdendritic liquid concentration $\langle C_d\rangle^d$, the growth rate of average instability is

$$\frac{\partial r_S^i}{\partial t} = \frac{0.75}{(r_S^i)(\lambda/2 - r_S^i)}\frac{A}{\langle C_d\rangle^d} \quad \text{where } A = \frac{\Gamma\,D_L}{m\,(k - 1)} \qquad \text{[IId]}$$

Expressing the average spacing λ in term of radius of average instability r_S^i and of internal fraction of solid f_i, the growth rate of average instability is further obtained as

$$\frac{\partial r_S^i}{\partial t} = \frac{0.75}{(r_S^i)^2}\frac{A}{\langle C_d\rangle^d}\frac{f_i^{1/3}}{(1 - f_i^{1/3})} \quad \text{with} \quad f_i = \frac{\langle v\rangle_S^i}{v_f^i}\,\phi_C = \frac{\langle v\rangle_S^i}{v_t^i} = \left(\frac{r_S^i}{\lambda/2}\right)^3 \qquad \text{[IIe]}$$

where v_f^i would be the final volume of average instability if there were no coarsening and v_f^i the actual (because of coarsening) volume of average instability (including the spacing around instability) at any time t during solidification.

Only for comparison with other coarsening models, Eq. [IIe] is written in term of λ, assuming that during solidification the instantaneous rate of coarsening is identical to the isothermal rate of coarsening,[21] *i.e.*, $\frac{1}{\lambda}\frac{\partial\lambda}{\partial t} = \frac{1}{r_S^i}\frac{\partial r_S^i}{\partial t}$. Then, Eq. [IIe] is expressed as

$$\lambda^2 \frac{\partial \lambda}{\partial t} = \frac{6A}{\langle C_d \rangle^d f_i^{2/3} (1 - f_i^{1/3})} \quad \text{or}$$
$$\frac{1}{\lambda} \frac{\partial \lambda}{\partial t} = \frac{6A}{\lambda^3 \langle C_d \rangle^d f_i^{2/3} (1 - f_i^{1/3})} \qquad [IIf]$$

ACKNOWLEDGMENTS

This work was partially supported by Grant No. NAGW—1192 from NASA through Auburn University and by the United States Department of Energy (DOE Cooperative Agreement No. DE-FC07-92ID13163). However, any opinions, findings, conclusions, or recommendations expressed herein are those of the authors and do not necessarily reflect the view of the DOE.

NOMENCLATURE

$\langle A \rangle$	surface area of the instability (m^2)
A	surface or interfacial area (m^2)
C	solute concentration (wt pct)
C_0	initial solute concentration (wt pct)
$\langle C_L \rangle^L$	intrinsic volume average extradendritic liquid concentration (wt pct)
$\langle C_d \rangle^d$	intrinsic volume average interdendritic liquid concentration (wt pct)
D	diffusion coefficient ($m^2\ s^{-1}$)
F_0	diffusive species transport number
G	gradient (km^{-1})
K_L	liquid thermal conductivity ($W\ m^{-1}\ K^{-1}$)
L	latent heat of fusion ($J\ kg^{-1}$)
MSI	microsegregation index
N_v	volumetric density (m^{-3})
N_j	number of instabilities
$\langle N \rangle$	average number of instabilities
$\dot{Q}$	rate of latent heat evolved ($J\ m^{-3}\ s^{-1}$)
Pe	Péclet number
R	tip radius (m)
R_E	radius of the equivalent dendrite envelope (m)
R_c	critical morphological radius (m)
R_n	nucleus radius (m)
R^*	radius of the equivalent dendrite volume (m)
S	specific interfacial area (m^{-1})
S_v	specific surface area (m^{-1})
T_b	bulk temperature (°C)
T_L	equilibrium liquidus temperature (°C)
T_m	melting temperature of the pure metal (°C)
$\dot{T}$	cooling rate ($°C\ s^{-1}$)
V	interface growth velocity (ms^{-1})
$\overline{V}$	average growth velocity (ms^{-1})
v	volume (m^3)
v_f	volume of element (m^3)
v_L	volume of liquid phase (m^3)
c_p	specific heat ($J\ kg^{-1}\ K^{-1}$)
f	volume fraction
h	heat transfer coefficient at the metal-mold interface ($W\ m^{-2}\ K^{-1}$)
k	equilibrium partition ratio
m	slope of the liquidus line ($K\ wt\ pct^{-1}$)
n	index number, number of series terms, or number of components in the alloy
r	radius coordinate (m)
r_S	dendrite arm radius (m)
v_f	final grain volume (m^3)
t	time (s)
t_f	solidification time (s)
x_s	solid volume distribution function
x, y, z	coordinates of the microelement within the macrosystem
Δv_j	incremental volume of a j instability
$\overline{\Delta v}$	incremental volume of the average instability
ΔT	undercooling (°C)
Δt	time-step (s)
ϕ_c	coarsening factor
μ	growth coefficient ($m\ s^{-1}\ K^{-2}$)
ρ	density ($kg\ m^{-3}$)
α_L	liquid thermal diffusivity ($m^2\ s^{-1}$)
α_n	nth root of $\alpha_n R_f \cot \alpha_n = R_f - R_E$
β	coarsening factor
λ_i	wavelength of instability (m)
λ_n	eigenvalue (characteristic value)
λ_2	secondary arm spacing (m)
σ^*	stability constant
Ω	supersaturation
Γ	Gibbs–Thomson coefficient (K m)
χ	shape factor
γ	interfacial surface energy, $J\ m^{-1}$

Subscripts/Superscripts

E	envelope
L	liquid or extradendritic liquid
s	solid
c	solutal
d	interdendritic
f	final
i	internal or instability
m	mush
t	thermal
$*$	at solid/liquid interface

REFERENCES

1. D.M. Stefanescu, G. Upadhya, and D. Bandyopadhyay: *Metall. Trans. A*, 1990, vol. 21A, pp. 997-1005.
2. M. Rappaz: *Int. Mater. Rev.*, 1989, vol. 34(3), pp. 93-123.
3. I. Maxwell and A. Hellawell: *Acta Metall.*, 1975, vol. 23, pp. 229-37.
4. I. Dustin and W. Kurz: *Z. Metallkd.*, 1986, vol. 77, pp. 265-73.
5. M. Rappaz and P. Thevoz: *Acta Metall.*, 1987, vol. 35, pp. 1487-97 and 2929-33.
6. C.Y. Wang and C. Beckermann: *Metall. Trans. A*, 1993, vol. 24A, pp. 2787-2802.
7. L. Nastac and D.M. Stefanescu: *Micro/Macro Scale Phenomena in Solidification*, ASME, Fairfield, NJ, 1992, HTD-vol. 218/AMD-vol. 139, pp. 27-34.
8. P. Thevoz, J.L. Desbiolles, and M. Rappaz: *Metall. Trans. A*, 1989, vol. 20A, pp. 311-22.
9. C.S. Kanetkar and D.M. Stefanescu: *AFS Trans.*, 1988, pp. 591-98.
10. C. Beckermann: in *Modeling of Casting, Welding, and Advanced Solidification Processes—VI*, T.S. Piwonka, W. Woller, and L. Katgerman, eds., TMS, Warrendale, PA, 1993, pp. 181-92.
11. J. Ni and C. Beckermann: *Metall. Trans. A*, 1991, vol. 22B, pp. 349-61.
12. E.E. Underwood: *Metals Handbook*, 9th ed., vol. 9, *Metallography and Microstructures*, ASM, Metals Park, OH, 1985, pp. 123-34.
13. W.W. Mullins and R.F. Sekerka: *J. Appl. Phys.*, 1963, vol. 34, pp. 323-29.
14. R.F. Sekerka: *Cryst. Growth*, 1973, pp. 403-43.
15. W. Kurz and D.J. Fisher: *Acta Metall.*, 1981, vol. 29, pp. 11-20.

16. L. Nastac and D.M. Stefanescu: *Metall. Trans. A*, 1993, vol. 24A, pp. 2107-18.
17. A. Roosz, E. Halder, and H.E. Exner: *Mater. Sci. Technol.*, 1986, vol. 2, pp. 1149-55.
18. T.Z. Kattamis and M.C. Flemings: *Trans. TMS-AIME*, 1967, vol. 233, p. 992.
19. U. Feurer and R. Wunderlin: *Fachbericht der Deutschen Gesselschaft fur Metallkunde*, Oberursel, Germany, 1977.
20. R.T. DeHoff: *Acta Metall.*, 1991, vol. 39 (10), pp. 2349-60.
21. A. Mortensen: *Metall. Trans. A*, 1991, vol. 22A, pp. 569-74.
22. S. Ahuja, C. Beckermann, R. Zakhem, P.D. Weidman, and H.C. deGroh III: *Micro/Macro Scale Phenomena in Solidification*, ASME, Fairfield, NJ, 1992, HTD-vol. 218/AMD-vol. 139, pp. 85-91.
23. H.C. deGroh III, P.D. Weidman, R. Zakhem, S. Ahuja, and C. Beckermann: *Metall. Trans. B*, 1993, vol. 24B, pp. 749-53.
24. D.R. Poirier: *Metall. Trans. B*, 1987, vol. 18B, pp. 245-55.
25. C. Beckermann and R. Viskanta: *Appl. Mech. Rev.*, 1993, vol. 46(1), pp. 1-27.
26. A.G. Guy, V. Leroy, and T.B. Lindemer: *Trans. ASM*, 1966, vol. 59, p. 517.
27. S. Kobayashi: *Trans. Iron Steel Inst. Jpn.*, 1988, vol. 28, pp. 535-41.
28. S. Kobayashi, T. Nagamichi, and K. Gunji: *Trans. Iron Steel Inst. Jpn.*, 1988, vol. 28, pp. 543-52.
29. A. Kagawa and T. Okamoto: in *Physical Metallurgy of Cast Iron*, H. Fredriksson and M. Hillert, eds., North-Holland, Amsterdam, 1985, p. 201.
30. F. Neumann: in *Recent Research on Cast Iron*, H.D. Merchant, ed., Gordon and Breach, New York, NY, 1968, p. 659.
31. T. Imwinkelried, J.L. Desboilles, Ch.A. Gandin, M. Rappaz, S. Rossman, and P. Thevoz: in *Modeling of Casting, Welding, and Advanced Solidification Processes VI*, T.S. Piwonka, V. Voller, and L. Katgerman, eds., TMS, Warrendale, PA, 1993, pp. 63-70.
32. M. Bobadilla, J. Lacaze, and G. Lesoult: *J. Cryst. Growth*, 1988, vol. 89, p. 531.
33. M.A. Chopra, M.E. Glicksman, and N.B. Singh: *Metall. Trans. A*, 1988, vol. 19A, pp. 3087-96.
34. J. Lipton, M.E. Glicksman, and W. Kurz: *Metall. Trans. A*, 1987, vol. 18A, pp. 341-45.
35. W. Kurz and D.J. Fisher: *Fundamentals of Solidification*, 2nd ed., Trans Tech Publications, Aedermannsdorf, Switzerland, 1986.
36. J.S. Kirkaldy: *Metall. Trans. A*, 1993, vol. 24A, pp. 1689-1721.
37. R. Ananth and W.N. Gill: *J. Cryst. Growth*, 1991, vol. 108, pp. 173-89.
38. L. Nastac and D.M. Stefanescu: *Metall. Mater. Trans. A*, 1996, vol. 27A, pp. 0000-00.
39. M.E. Glicksman, R.J. Schaefer, and J.D. Ayers: *Metall. Trans. A*, 1976, vol. 7A, pp. 1747-59.
40. H.B. Aaron, D. Fainstein, and G.R. Kotler: *J. Appl. Phys.*, 1970, vol. 41 (11), pp. 4405-09.